发 光 学 报
CHINESE JOURNAL OF LUMINESCENCE

Article ID: 1000-7032(XXXX)XX-0001-10

Pyridylamine-Driven Interfacial Passivation via Coordination and Hydrogen Bonding Enables Efficient Perovskite Solar Cells

CHEN Xin[1], HU Li-hua[1], ZHANG Zuo-lin[2*], CUI Hong-jun[3*], CHEN Cong[2,4,5*]

(1. *Hebei Expressway Group Zhuoneng Co., Ltd, Zhangjiakou* 076150, *China*;
2. *State Key Laboratory of Smart Power Distribution Equipment and System, School of Materials Science and Engineering, Hebei University of Technology, Tianjin* 300401, *China*;
3. *School of Civil and Transportation Engineering, Hebei University of Technology, Tianjin* 300401, *China*;
4. *Science and Technology on Advanced Ceramic Fibers and Composites Laboratory, National University of Defense Technology, Changsha* 410073, *China*;
5. *Shandong Jiusi New Material Technology Co., Ltd, Jining* 273200, *China*)

* *Corresponding Authors, E-mail: zuolin*2024@126. *com* (*Z. Z*), *cuihongjun@hebut. edu. cn* (*H. C*); *chencong@hebut. edu. cn* (*C. C*)

Abstract: PSCs (PSCs) have garnered significant attention for their high efficiency, but their commercial application is hindered by stability issues caused by defects such as uncoordinated Pb^{2+} ions and halide vacancies. This work introduces 3-amino-2,6-dichloropyridine (ADCP) as a novel pyridylamine additive for PSCs, aiming to enhance both device efficiency and stability. ADCP features a pyridine functional group that coordinates with Pb^{2+} ions and forms hydrogen bonds with halide ions, enabling dual-site passivation of defects. This dual interaction reduces Pb-related defects, improves crystallinity, and enhances charge transport within the perovskite layer. The devices exhibit a PCE of 25. 59%, with significant improvements in long-term stability, maintaining 81% of the initial PCE for nearly 500 hours. The study highlights the effectiveness of pyridylamine-driven passivation in overcoming stability issues and enhancing the overall performance of PSCs, providing a promising strategy for high-efficiency, stable perovskite photovoltaics.

Keywords: Perovskite solar cells; Hydrogen bonding; Pyridylamine
CLC number: TM914. 4 **Document code**: A
DOI: 10. 37188/CJL. 20260036 **CSTR**: 32170. 14. CJL. 20260036

吡啶胺驱动的配位与氢键界面钝化实现高效钙钛矿太阳能电池

陈 昕[1], 胡利华[1], 张左林[2*], 崔洪军[3*], 陈 聪[2,4,5*]

(1.河北高速公路集团卓能有限公司, 中国张家口 076150;
2.智能配用电装备与系统全国重点实验室,河北工业大学材料科学与工程学院, 中国天津 300401;
3.河北工业大学土木与交通学院, 中国天津 300401;
4.新型陶瓷纤维及其复合材料国防科技重点实验室,国防科技大学, 中国长沙 410073;
5.山东九思新材料科技有限公司, 中国济宁 273200)

收稿日期: 2020-01-03; **修订日期**: 2020-01-05
基金项目: 河北高速公路集团有限公司科技创新项目(No. 1906536076810387456);国家自然科学基金(52473257);山东省泰山产业创新领军人才项目(NO. tscx202312156)资助
Supported by the Hebei Expressway Group Zhuoneng Co., Ltd. Technology Innovation Project (No. 1906536076810387456). The National Natural Science Foundation of China (52473257). The Taishan Industrial Experts Program (NO. tscx202312156).

摘要：钙钛矿太阳能电池(PSCs)因其优异的光电转换效率而备受关注，但未配位Pb^{2+}离子与卤素空位等本征缺陷所诱发的非辐射复合与离子迁移，仍显著制约其长期运行稳定性与商业化进程。本研究提出3-氨基-2，6-二氯吡啶(ADCP)作为新型吡啶胺类添加剂，用于协同提升器件效率与稳定性。ADCP同时包含可与Pb^{2+}配位的吡啶氮位点以及可与卤素阴离子形成氢键的氨基官能团，从而实现对缺陷的“双位点”化学钝化与晶格稳定：一方面削弱Pb相关深能级陷阱并降低缺陷密度，另一方面促进薄膜结晶质量提升与界面电荷传输/抽取优化。基于该策略构筑的器件获得25.59%的光电转换效率(PCE)，并表现出显著增强的长期稳定性，在近500小时的测试周期内仍可保持初始PCE的81%。本工作表明，吡啶胺驱动的“配位—氢键”协同钝化为缓解PSCs稳定性瓶颈、构筑高效率且可持续运行的钙钛矿光伏器件提供了一条具有普适性的分子设计与界面调控路径。

关 键 词：钙钛矿太阳能电池；氢键；吡啶胺

1 Introduction

Perovskite solar cells (PSCs) have rapidly emerged as one of the most promising candidates for high-efficiency photovoltaic devices, largely due to their exceptional optoelectronic properties, such as high absorption coefficients, tunable band gaps, and long carrier diffusion lengths. [1-6] These unique properties have contributed to a significant increase in the PCE exceeding 27% of PSCs[7, 8], making them a compelling alternative to traditional silicon-based photovoltaics. However, despite these advances, PSCs still face considerable challenges, particularly related to the intrinsic defects present in the perovskite layer[9-14]. These include uncoordinated Pb^{2+} ions, halide vacancies, and poor crystallinity, all of which contribute to nonradiative recombination, reduced charge transport efficiency, and lower device performance[15-17]. Moreover, the inherent instability of perovskite materials—exacerbated by factors such as ion migration, moisture, UV light, and heat—further limits their widespread commercial application[18-20].

One promising strategy for overcoming the defects induced by uncoordinated Pb^{2+} ions is the passivation of defects in the perovskite layer using molecular additives. [1, 21-27] Among various defect passivation methods, pyridine-functionalized organic molecules have garnered significant attention due to their unique ability to coordinate with Pb^{2+} ions[28]. The nitrogen atom within the pyridine ring forms a stable coordination bond with Pb^{2+} ions, which effectively neutralizes the detrimental effects of uncoordinated Pb^{2+} defects that are commonly found at the surface and grain boundaries of perovskite films. This coordination significantly reduces the recombination rates associated with these defects, leading to enhanced charge carrier mobility and improved device performance. Furthermore, pyridine-based molecules have been shown to facilitate the formation of a passivation layer on the perovskite surface, which reduces surface traps and enhances the stability of PSCs under operational conditions.

In recent years, incorporating functional ligands into PSCs has emerged as an effective route to alleviate Pb-related concerns, largely by enabling robust defect passivation through ligand - perovskite hydrogen-bonding interactions between specific functional groups and the perovskite lattice. Among various defect passivation strategies, molecular additives capable of forming stable coordination bonds with Pb^{2+} ions and hydrogen bonds (H-bonds) with halide ions synchronously have shown more promise in enhancing both the stability and performance of PSCs[29]. Hydrogen bonding[30-32], in particular, has been identified as a crucial interaction for stabilizing perovskite films. It not only helps improve the structural integrity of the perovskite material but also prevents ion migration, which can degrade the device performance under environmental stress. For example, Li et al. [33] demonstrated the effectiveness of hydrogen bonding and coordination in stabilizing PSCs with conjugated organic molecules, highlighting how these interactions significantly improve both the efficiency

and long-term stability by passivating defects, particularly Pb^{2+} ions, and preventing their migration. Also, Bai et al. [34] demonstrated that hydrogen bonding interactions between the crosslinkable silane-functionalized fullerene and the perovskite layer significantly enhance the stability and efficiency of PSCs, showing how these hydrogen bonds help reduce defect density and prevent moisture-induced degradation, ultimately improving both the device performance and long-term stability.

Considering the need for simultaneous passivation of undercoordinated Pb^{2+} defects and stabilization of the perovskite lattice via hydrogen bonding, pyridylamine-based molecules are promising candidates for synergistic defect regulation. Here, we introduce 3-amino-2, 6-dichloropyridine (ADCP) as a rationally designed dual-functional additive for PSCs. Distinct from conventional pyridine- or amine-based passivators, ADCP integrates a pyridinic nitrogen, an amino group, and two electron-withdrawing chloro substituents at the 2,6-positions, enabling strengthened and cooperative molecular interactions with the perovskite lattice. The amino group forms hydrogen bonds with halide ions, particularly iodide, helping to stabilize the lattice and suppress halide migration, while the pyridinic nitrogen strongly coordinates with undercoordinated Pb^{2+} ions, effectively passivating deep-level trap states. The electron-withdrawing dichloro substituents further enhance the interaction strength of the pyridine moiety, leading to more robust defect suppression compared with previously reported mono-functional additives. Through this synergistic dual interaction, ADCP reduces defect density at the surface and grain boundaries, improves interfacial contact, and facilitates charge transport, resulting in suppressed nonradiative recombination, enhanced carrier extraction, improved operational stability, and ultimately higher device efficiency. This work demonstrates that rational molecular design of ADCP enables simultaneous chemical passivation and interfacial regulation, providing an effective strategy for achieving efficient and stable PSCs.

2 Experiment

2.1 Materials

Formamidine iodide (FAI, 99.5%) and methylammonium chloride (MACl, 99.5%) were purchased from Greatcell Solar Materials. Lead iodide (PbI_2, 99.999%) and cesium iodide (CsI, 99.99%) were purchased from Chengdu Alfa Metal Materials Co., Ltd. N, N-dimethylformamide (DMF, 99.9%), isopropanol (IPA, suitable for HPLC, 99.9%), and dimethyl sulfoxide (DMSO, 99.9%) were purchased from Sigma-Aldrich. BCP, $PC_{61}BM$, and C_{60} were purchased from Advanced Election Technology. [4-(3, 6-Dimethyl-9H-carbazol-9-yl)butyl]phosphonic acid (Me-4PACz, 99.0%) was purchased from TCI. ADCP (98%) was purchased from Macklin.

2.2 Fabrication of PSCs

The ITO glass substrates were cleaned with a detergent solution, deionized water, acetone, and anhydrous ethanol for 10 min, respectively. Next, the substrates were further cleaned with plasma treatment for 10 min. Then, NiO_x films were fabricated by spin-coating the 5 mg/mL NiO_x aqueous solution on the ITO substrates at 4000 rpm for 20 s, followed by annealing at 150 °C for 10 min. Then, 0.5 mg/mL Me-4PACz ethanol solution was spin-coated on NiO_x film at 4000 rpm for 30 s, followed by annealing at 100 °C for 10 min. The 1.53 eV $Cs_{0.05}FA_{0.95}PbI_3$ perovskite precursors were dissolved with 5 mol% MACl in a mixed DMF and DMSO solvent (4:1 v/v) at a concentration of 1.4 M. For the ADCP-modified devices, 1, 2, and 3 mg of ADCP were added to 1 mL of perovskite precursor solution. Among them, 2 mg of ADCP yielded the optimal enhancement in PCE, V_{OC}, J_{SC}, and FF, indicating that this concentration provides the best improvement in device performance (**Fig.** 3b). Subsequently, the perovskite films were deposited by spin-coating the perovskite precursor solution on Me-4PACz/NiO_x/ITO/glass substrate at 4000 rpm for 30 s. The wet perovskite film was quickly put into a sample chamber connected to vacuum-pumping instrumentation. By opening the valve connecting the specimen chamber to the pump system, the perovskite film was im-

mediately exposed to low pressure maintained at 10 Pa for 40 seconds, followed by full pressurization by admitting ambient air into the specimen chamber. Subsequently, the perovskite film was annealed at 100 °C for 10 minutes. 20 nm of C_{60} and 5 nm of BCP were deposited by thermal evaporation. Finally, 100 nm of Ag counter electrode was thermally evaporated under a high vacuum.

2.3 Measurements and Characterization

The *J*–*V* characterizations were measured by a Keithley 2400 source under simulated AM 1.5 irradiation with a standard xenon-lamp-based solar simulator (7ISO503A, SOFN INSTRUMENTS). EIS measurement was performed in the dark by AMETEK VersaSTAT 3F at a frequency from 1 Hz to 1 MHz. Mott-Schottky measurement was done by using the same instrument as used in EIS, but at a fixed frequency of 1 kHz. The applied bias voltage range is 0 to 1.5 V. TPC/TPV was tested by PD-RS of ENLITECH, Taiwan. The ultraviolet-visible absorption spectra of the films were measured using a Shimazu UV-1900 spectrophotometer.

3 Results and Discussion

Fig. 1a presents the chemical structure of 3-amino-2, 6-dichloropyridine (ADCP), which consists of a pyridine ring substituted with two chlorine atoms and an amino group ($-NH_2$). The amino group is crucial for interacting with halide ions (I^-) through hydrogen bonding, while the nitrogen atom in the pyridine ring can coordinate with Pb^{2+} ions. This dual functionality of ADCP makes it a promising candidate for defect passivation in perovskite materials, particularly targeting the Pb^{2+} and halide defects commonly found in PSCs. As shown in **Fig.** 1b, the interaction between ADCP and the perovskite crystal structure is depicted. The amino group in ADCP forms hydrogen bonds with iodide ions (I^-), while the nitrogen atom coordinates with Pb^{2+} ions within the perovskite lattice. This coordination mechanism is essential for passivating the uncoordinated Pb^{2+} defects present at the surface and grain boundaries of perovskite films. By reducing these defects, ADCP improves the crystallinity and stability of the perovskite layer, which is crucial for enhancing the overall performance and longevity of PSCs.

As shown from the absorbance spectra of ADCP, FAI (formamidinium iodide), and the combination of FAI and ADCP in **Fig.** 1c, it can be seen that the ADCP samples display a distinctive peak, while the FAI spectrum shows a broader absorption feature. When ADCP is mixed with FAI, a shift in the absorption spectrum is observed, indicating that ADCP interacts with FAI, likely through the coordination of its amino and nitrogen groups. This interaction is important because it suggests that ADCP modifies the electronic properties of the perovskite precursor, which can influence the crystallization process and the optical characteristics of the resulting perovskite films. **Fig.** 1d demonstrates the absorbance spectra of ADCP, PbI_2, and the mixture of PbI_2 and ADCP. The addition of ADCP to PbI_2 causes a shift in the absorption peaks, particularly in the region of 400 – 500 nm. This shift indicates that ADCP forms a stable complex with Pb^{2+} ions, as evidenced by the changes in the spectral features. The coordination between ADCP and Pb^{2+} is crucial for passivating Pb-related defects in the perovskite structure. This interaction reduces defect-related recombination and stabilizes the perovskite film, enhancing the overall efficiency and stability of the solar cells fabricated with these materials.

The crystallization quality of the perovskite films was further investigated by SEM and XRD measurements. As shown in **Fig.** 1e and f, the control film exhibits relatively small grains and a less uniform surface, whereas the ADCP-modified film presents enlarged grains and a more compact and homogeneous morphology with fewer visible pinholes. This indicates that ADCP incorporation promotes more uniform crystal growth and suppresses defect formation during film formation. Consistently, the XRD patterns shown in **Fig.** 1g reveal that the ADCP-modified film displays stronger diffraction intensity compared with the control, suggesting enhanced crystallinity and improved crystal quality. The absence of additional impurity peaks also indicates

that ADCP incorporation does not disrupt the perovskite phase. These results collectively confirm that ADCP doping effectively improves the crystalline quality of the perovskite films.

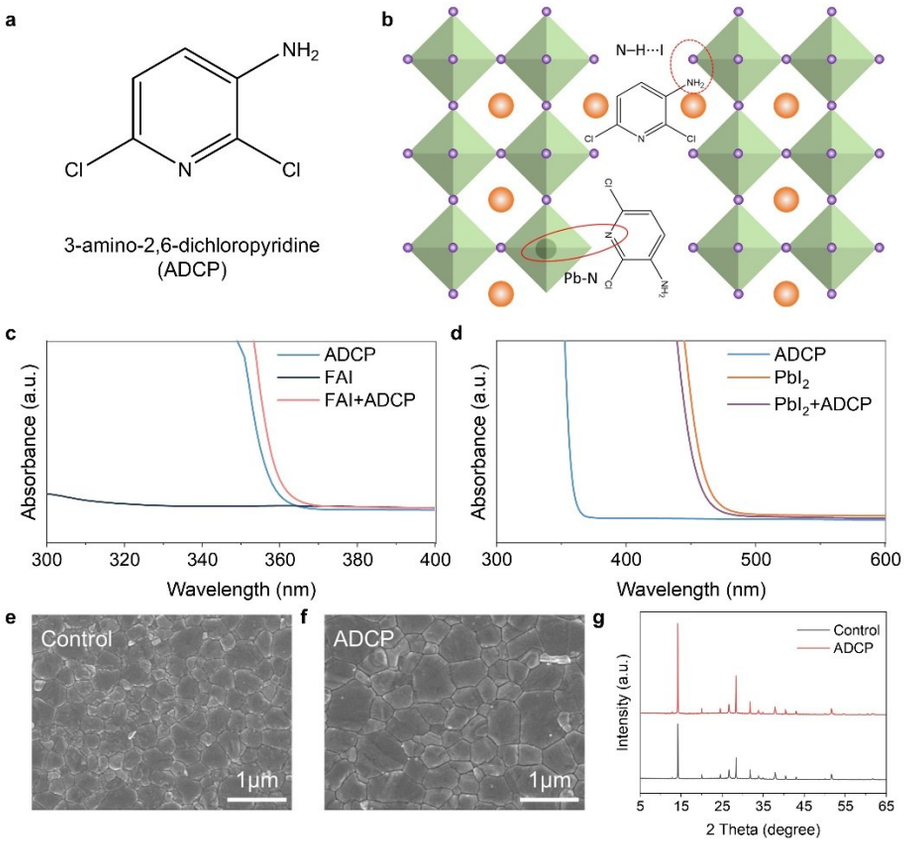

图 1 (a) ADCP的化学结构(作为修饰剂);(b) ADCP与钙钛矿晶体之间的相互作用示意图;(c) ADCP及FAI/ADCP混合物的吸收光谱;(d) ADCP及PbI2/ADCP混合物的吸收光谱;(e, f) 钙钛矿薄膜的俯视SEM图像,分别为对照组和ADCP修饰薄膜;(g) 引入ADCP前后钙钛矿薄膜的XRD衍射图谱。

Fig. 1 (a) Chemical Structure of ADCP as modifier; (b) Interaction between ADCP and perovskite crystals; (c) Absorbance spectrum of ADCP and FAI/ADCP mixture; (d) Absorbance spectrum of ADCP and PbI_2/ADCP mixture. Top-view SEM images of perovskite films: (e) Control and (f) ADCP-modified films. (g) XRD patterns of perovskite films before and after ADCP incorporation.

The fabricated processes To verify the impact of the ADCP-enabled pyridylamine-driven interfacial passivation via coordination and hydrogen bonding strategy on charge-transport characteristics in PSCs, we performed a series of electrical characterizations and systematic analyses. **Fig.** 2a presents capacitance-voltage (C-V) measurements of PSCs with and without ADCP. The control device shows higher capacitance at lower voltages, indicating the presence of more trap states and a higher defect density, which limits charge transport. In contrast, the ADCP-modulated device exhibits a significant reduction in capacitance, especially below 0.8 V, where it stabilizes at a lower value of 6×10^{16} $1/F^2$ compared to 10×10^{16} $1/F^2$ for the control. This reduction indicates that ADCP effectively passivates surface defects, improving charge transport efficiency. From the Nyquist plots derived from electrochemical impedance spectroscopy (EIS) in **Fig.** 2b, the ADCP-modulated device exhibits a smaller semicircular arc and lower impedance (3.5 kΩ vs. 7.5 kΩ in the control), confirming that ADCP enhances electron mobility and reduces resistance at the perovskite/electron transport layer interface.

Fig. 2c-d present time-resolved photocurrent (TPC) and photovoltage (TPV) decay profiles, respectively. The TPC decay of the control device shows a rapid decay with a time constant of 0.156 μs, indi-

cating significant charge carrier recombination. In contrast, the ADCP-modulated device demonstrates a slower decay (0.198 μs), suggesting reduced recombination and enhanced carrier retention. This slower decay, along with an increased photocurrent, shows that ADCP improves charge collection efficiency and minimizes recombination losses. Similarly, in the TPV decay measurement, the control device shows rapid voltage decay with a time constant of 2.638 ms, indicative of faster recombination. The ADCP-modulated device exhibits a slower decay with a time constant of 3.782 ms, signifying that ADCP enhances charge retention by reducing recombination.

To further investigate the interfacial charge transfer dynamics, steady-state PL and TRPL measurements were performed on SAM/PVSK/C_{60} structures. As shown in **Fig.** 2e and 2f, the ADCP-modified film exhibits significantly quenched PL intensity and a faster TRPL decay compared with the control sample. The pronounced PL quenching indicates that photogenerated electrons are more efficiently extracted from the perovskite into the C_{60} layer rather than undergoing radiative recombination within the perovskite film. Meanwhile, the shortened PL lifetime is attributed to accelerated interfacial charge transfer rather than increased nonradiative recombination. These results demonstrate that ADCP incorporation not only contributes to defect passivation but also improves interfacial contact and energy-level alignment, thereby facilitating charge extraction and suppressing interfacial recombination losses.

These results demonstrate that ADCP not only improves charge transport but also contributes to long-term device stability and efficiency by passivating defects.

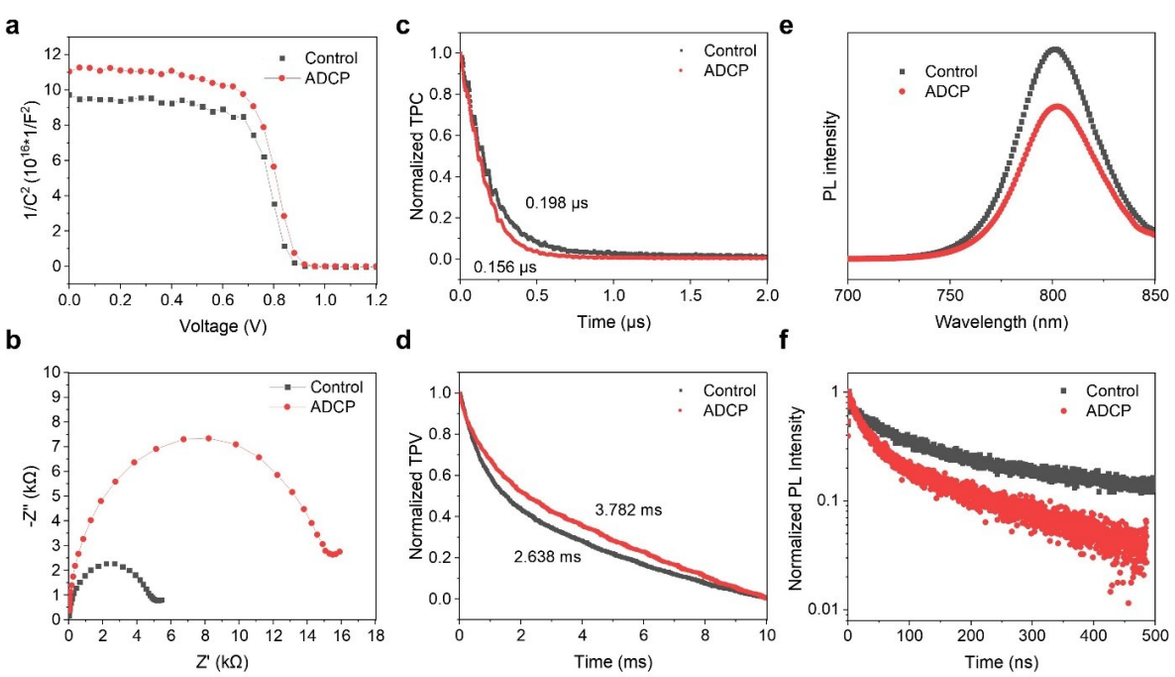

图 2 对照组与 ADCP 修饰 PSC 的电学性能表征:(a) 对照器件与 ADCP 器件的 Mott - Schottky 曲线(1/C2 - V);(b) 电化学阻抗谱的 Nyquist 图;(c) 瞬态光电流(TPC)衰减曲线;(d) 瞬态光电压(TPV)衰减曲线;ITO/SAM/钙钛矿/C60 薄膜在有无 ADCP 调控下的(e) PL 和(f) TRPL 光谱。

Fig. 2 Electrical characterizations of control and ADCP-modified PSCs. (a) Mott - Schottky plots ($1/C^2$ - V) of control and ADCP devices. (b) Nyquist plots from EIS. (c) TPC decay curves. (d) TPV decay curves. (e) PL and (f) TRPL spectra of the ITO/SAM/perovskite/C_{60} films with and without ADCP modulation.

The device architecture of the ADCP-modulated PSCs is shown in **Fig.** 3a. The structure follows a standard planar heterojunction configuration, starting with a transparent conductive oxide (ITO) substrate, followed by a NiOx and Me-4PACz as hole transport layer (ETL). The perovskite layer, which

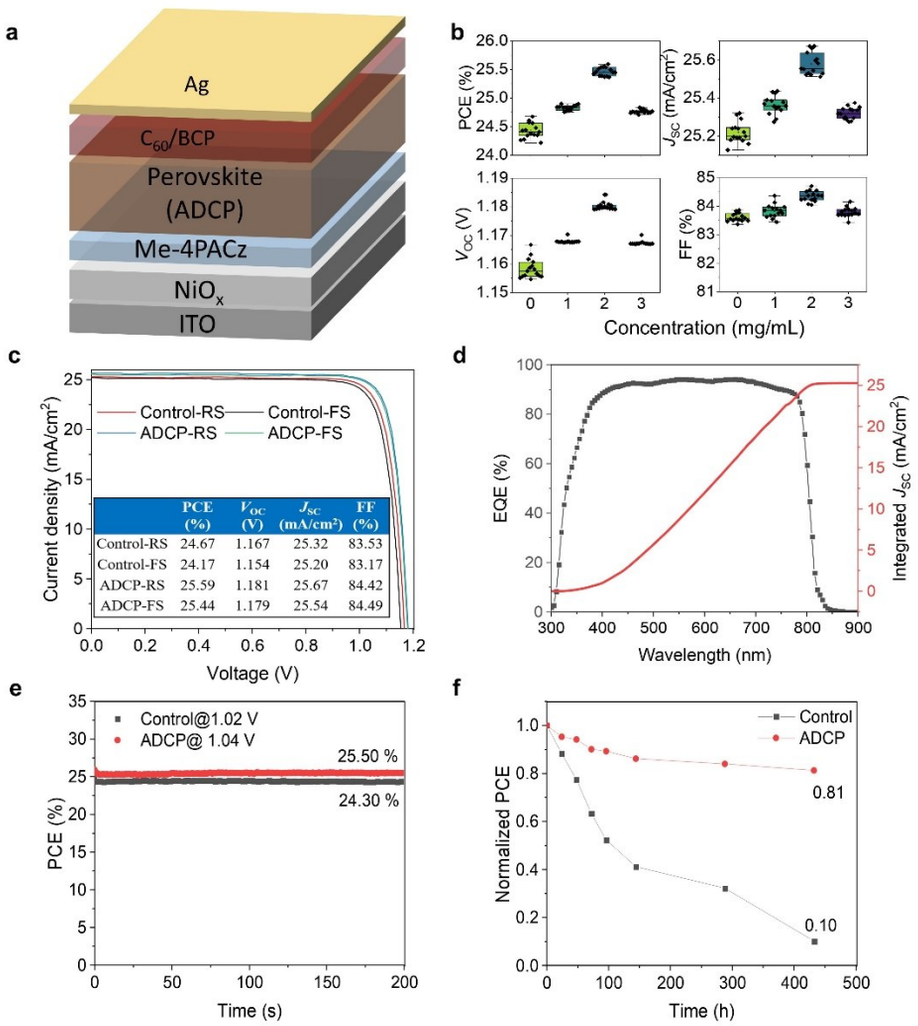

图 3 (a) ADCP 调控 PSC 的器件结构示意图;(b) ADCP 调控 PSC 性能随 ADCP 浓度变化的关系;(c) 对照组与 ADCP 调控 PSC 器件在反向扫描(RS)和正向扫描(FS)模式下的 J - V 特性曲线;(d) ADCP 修饰 PSC 的 EQE 光谱;(e) ADCP 调控器件与对照器件在连续光照老化条件下的 PCE 稳定性;(f) ADCP 调控器件与对照器件的长期稳定性,器件在约 25 °C、相对湿度 40 - 60% 的环境空气中、未封装条件下储存。

Fig. 3 (a) Schematic diagram of the device architecture for ADCP-modulated PSCs. (b) Performance of ADCP-modulated PSCs as a function of ADCP concentration. (c) *J–V* characteristics of the control and ADCP-modulated PSC devices under RS and FS modes. (d) EQE spectra of the ADCP-modified PSCs. (e) PCE stability of ADCP-modulated and control devices under continuous light soaking. (f) Long-term stability of the ADCP-modulated and control devices. Stored under ambient atmosphere with ~25 °C temperature and 40 - 60% relative humidity, without encapsulation.

includes the ADCP passivation additive, is sandwiched between the hole transport layer (NiOx/Me-4PACz) and the C_{60}/BCP buffer layer. Finally, a silver (Ag) electrode is deposited on top to complete the device. This configuration ensures efficient charge extraction and reduces recombination at the interfaces, thereby enhancing the overall performance of the device. The fabrication process of the PSCs involves vacuum flash evaporation, completed in an ambient environment. In **Fig.** 3b, the performance of the ADCP-modulated PSCs is shown as a function of ADCP concentration. The devices exhibit a clear trend of improving PCE as the ADCP concentration increases, reaching an optimal PCE at 2 mg/mL. The best-performing devices, with an optimized concentration of 2 mg/mL, achieve a best PCE of 25. 59%. At concentrations higher than 2 mg/mL, the efficiency slightly decreases, which suggests that an optimal concentration exists where the ADCP concentration maximizes defect passivation without in-

troducing excessive molecular aggregation or interference with the perovskite crystallization.

The $J-V$ curves for the ADCP-modulated PSCs and the control devices, shown in **Fig.** 3c, highlight the improvements in charge transport and collection efficiency due to the ADCP treatment. The ADCP-modulated devices show higher J_sc values and improved fill factors (FF), resulting in higher PCEs. Specifically, the ADCP-modulated devices exhibit a J_{SC} of 25.67 mA/cm^2 (ADCP-RS) and 25.54 mA/cm^2 (ADCP-FS), compared to 25.32 mA/cm^2 (Control-RS) and 25.20 mA/cm^2 (Control-FS) for the control devices. The fill factor (FF) also increases from 83.53% in the control devices to 84.42% (ADCP-RS) and 84.49% (ADCP-FS), further confirming the improvement in the device efficiency. The photovoltaic performance of the ADCP-modified device was further verified by external quantum efficiency (EQE) measurement. As shown in **Fig.** 3d, the integrated current density calculated from the EQE spectrum reached 25.285 mA cm^{-2}, which is in good agreement with the J_{SC} value obtained from the $J-V$ measurement. **Fig.** 3e shows the PCE stability of the ADCP-modulated and control devices under continuous light soaking. The ADCP-modulated devices (both ADCP-RS and ADCP-FS) maintain a higher PCE, stabilizing at 25.50% after 200 seconds of light exposure, compared to the control devices, which decrease to 24.30%. This demonstrates that the ADCP passivation not only improves initial efficiency but also enhances the long-term stability of the devices, making them more resilient to light-induced degradation.

In **Fig.** 3f, the long-term stability of the ADCP-modulated and control devices is shown by monitoring the normalized PCE for nearly 500 hours. The ADCP-modulated devices retain 81% of their initial PCE after 500 hours, whereas the control devices maintain only 10%. This substantial improvement in stability confirms the efficacy of ADCP in reducing the defect density at the interface, which significantly prolongs the operational lifetime of the PSCs. Thus, the ADCP-modulated PSCs exhibit improved efficiency, stability, and long-term performance, with an optimal concentration of ADCP at 2 mg/mL providing the best results. These enhancements demonstrate the potential of ADCP as a valuable additive for PSCs, facilitating efficient defect passivation and leading to superior device performance.

4 Conclusion

In conclusion, this work demonstrates the effectiveness of ADCP as a dual-functioning pyridylamine additive for PSCs. By coordinating with Pb^{2+} ions and forming hydrogen bonds with halide ions, ADCP efficiently passivates defects, improving crystallinity, charge transport, and stability. The ADCP-modulated PSCs exhibit a notable efficiency of 25.59% and exceptional long-term stability, maintaining 81% of their initial PCE for nearly 500 hours. This research highlights the potential of pyridylamine-driven passivation to address both efficiency and stability challenges in PSCs, providing a promising strategy for developing more robust and high-performance perovskite photovoltaics.

Response Letter is available for this paper at:http://cjl.light-publishing.cn/thesisDetails#10.37188/CJL.20260036.

References:

[1] LI M, DING J, ZHANG Z, *et al*. Functional Group Engineering Stabilizing Precursor Solution and Passivating Defects for Operationally Stable and Highly Reproducible Inverted Perovskite Solar Cells [J]. *Adv Mater*, 2025, 37(27): 2502729.

[2] ZHANG Z, DING J, LIU H, *et al*. Immobilizing Lead and Healing Surface Defects via Perfluorinated Tertiary Amine Molecules Enables High-Performance Sustainable Inverted Perovskite Solar Cells [J]. *Adv Mater*, 2025, 37(39): 2508126.

[3] DING J, LIAO Y, LIU H, *et al*. Stabilizing buried interface by bilateral bond strength equilibrium strategy toward efficient perovskite photovoltaics [J]. *Nat Commun*, 2025, 16(1): 8407.

[4] CHEN P, XIAO Y, HU J, *et al*. Multifunctional ytterbium oxide buffer for perovskite solar cells [J]. *Nature*, 2024, 625

(7995): 516-22.

[5] JIANG W, QU G, HUANG X, *et al.* Toughened self-assembled monolayers for durable perovskite solar cells [J]. *Nature*, 2025, 646(8083): 95-101.

[6] KAN C, HANG P, WANG S, *et al.* Efficient and stable perovskite-silicon tandem solar cells with copper thiocyanate-embedded perovskite on textured silicon [J]. *Nature Photonics*, 2025, 19(1): 63-70.

[7] LU H, ZHUANG X, DING J, *et al.* Ion-Defect Dual Management for Achieving Efficient Air-Processed Perovskite Solar Cells With Certified Efficiency 27.1% [J]. *Advanced Materials*, 2026: e17596.

[8] XIONG Z, ZHANG Q, CAI K, *et al.* Homogenized chlorine distribution for >27% power conversion efficiency in perovskite solar cells [J]. *Science*, 2025, 390(6773): 638-42.

[9] WANG K, YANG D, WU C, *et al.* Mono-crystalline Perovskite Photovoltaics toward Ultrahigh Efficiency? [J]. *Joule*, 2019, 3(2): 311-6.

[10] GUO Y, HUANG H, ZHANG Y, *et al.* Molecular locking of defects via H-bonding/coordination dual-interaction enables efficient perovskite solar cells [J]. *Journal of Materials Chemistry A*, 2025, 13(32): 26564-72.

[11] DING B, DING Y, PENG J, *et al.* Dopant-additive synergism enhances perovskite solar modules [J]. *Nature*, 2024, 628(8007): 299-305.

[12] JIA L, XIA S, LI J, *et al.* Efficient perovskite/silicon tandem with asymmetric self-assembly molecule [J]. *Nature*, 2025, 644(8078): 912-919

[13] LI J, DUAN J, ZHANG C, *et al.* Facet-orientation-enhanced thermal transfer for temperature-insensitive and stable p-i-n perovskite solar cells [J]. *eScience*, 2025: 100372.

[14] 姚广平,文超,刘佳澎等. 缺陷对全无机钙钛矿太阳能电池性能的影响[J]. 发光学报,2023,44(11):2033-2040.
YAO G, WEN C, LIU J, *et al.* Effect of Defects on Performance of All Inorganic Perovskite Solar Cells[J]. *Chinese Journal of Luminescence*, 2023, 44(11): 2033-2040.

[15] ZHENG X, CHEN B, DAI J, *et al.* Defect Passivation in Hybrid Perovskite Solar Cells using Quaternary Ammonium Halide Anions and Cations [J]. *Nature Energy*, 2017, 2(7): 17102.

[16] LIANG Z, XU H, HUANG Z, *et al.* Suppression of PCBM dimer formation in inverted perovskite solar cells [J]. *Nature Materials*, 2025, 25, 267–274

[17] MA C, EICKEMEYER F T, LEE S-H, *et al.* Unveiling facet-dependent degradation and facet engineering for stable perovskite solar cells [J]. *Science*, 2023, 379(6628): 173-8.

[18] WANG D, LI Y, YANG Y, *et al.* Energetic disorder dominates optical properties and recombination dynamics in tin-lead perovskite nanocrystals [J]. *eScience*, 2025, 5(1): 100279.

[19] ZHU A, CHEN L, ZHANG A, *et al.* Playdough-like carbon electrode: A promising strategy for high efficiency perovskite solar cells and modules [J]. *eScience*, 2024, 4(2): 100221.

[20] 许振桐,林杰,HUANG Jingsong等. 大面积钙钛矿太阳能电池薄膜制备工艺进展综述[J]. 发光学报,2025,46(01):98-109.
XU Z, LIN J, HUANG J, *et al.* Review of Advances in Large-area Perovskite Solar Cell Thin-film Fabrication Techniques [J]. *Chinese Journal of Luminescence*, 2025, 46(01): 98-109.

[21] ZHU L, ZHANG X, LI M, *et al.* Trap State Passivation by Rational Ligand Molecule Engineering toward Efficient and Stable Perovskite Solar Cells Exceeding 23% Efficiency [J]. *Adv Energy Mater*, 2021, 11(20): 2100529.

[22] LI Y, ZHANG Z, CAI Y, *et al.* Synergistic Isothiourea–Guanidine Additive for Achieving Stable Perovskite Solar Cells with a High Certified Quasi-Steady-State Output [J]. *Adv Mater*, 2026, 38(3): e14903.

[23] SU Y, DING J, ZHANG Z, *et al.* Chemical inhibition of light-induced decomposition by hindered amine for efficient and stable perovskite solar cells [J]. *eScience*, 2025, 6(1): 100451.

[24] KIM M, KIM G-H, LEE T K, *et al.* Methylammonium Chloride Induces Intermediate Phase Stabilization for Efficient Perovskite Solar Cells [J]. *Joule*, 2019, 3(9): 2179-92.

[25] JEONG J, KIM M, SEO J, *et al.* Pseudo-halide anion engineering for α-FAPbI3 perovskite solar cells [J]. *Nature*, 2021, 592(7854): 381-5.

[26] SHI P, DING Y, DING B, *et al.* Oriented nucleation in formamidinium perovskite for photovoltaics [J]. *Nature*, 2023, 620(7973): 323-7.

[27] 侯昱,刘金龙,许鹤等. 多功能乳清酸钝化协助制备高效稳定的钙钛矿太阳能电池[J]. 发光学报,2024,45(08):1364-1370.
HOU X,LIU J,XU H,*et al*. Multifunctional Orotic Acid Passivation for Efficient and Stable Perovskite Solar Cells[J]. *Chinese Journal of Luminescence*,2024,45(08):1364-1370.

[28] CHENG H, ZANG X, WANG S, *et al*. Pyridine-Functionalized Organic Molecules in Perovskite Solar Cells: Toward Defects Passivation and Charge Transfer [J]. *Solar RRL*, 2025, 9(2): 2400736.

[29] AHMED R, REHMAN S, CHEN Z, *et al*. Ligand Assisted Hydrogen Bonding: A Game-Changer in Lead Passivation and Stability in Perovskite Solar Cells [J]. *Angewandte Chemie*, 2025, 137(2): e202418763.

[30] MENG X, LIN J, LIU X, *et al*. Highly Stable and Efficient FASnI3-Based Perovskite Solar Cells by Introducing Hydrogen Bonding [J]. *Advanced Materials*, 2019, 31(42): 1903721.

[31] TIAN C, SUN A, ZHUANG R, *et al*. Minimizing Interfacial Energy Loss and Volatilization of Formamidinium via Polymer-Assisted D - A supramolecular Self-Assembly Interface for Inverted Perovskite Solar Cells with 25.78% Efficiency [J]. *Advanced Materials*, 2024, 36(36): 2404797.

[32] LI F, DENG X, SHI Z, *et al*. Hydrogen-bond-bridged intermediate for perovskite solar cells with enhanced efficiency and stability [J]. *Nature Photonics*, 2023, 17(6): 478-84.

[33] LI T, ZHU T, ZHANG X, *et al*. Stable and efficient perovskite solar cells via hydrogen bonding and coordination [J]. *Nanoscale*, 2023, 15(48): 19557-68.

[34] BAI Y, DONG Q, SHAO Y, *et al*. Enhancing stability and efficiency of perovskite solar cells with crosslinkable silane-functionalized and doped fullerene [J]. *Nature Communications*, 2016, 7(1): 12806.

陈昕(1973-),男,湖南大学学士,正高级经济师,河北高速公路集团有限公司张承张家口分公司(延崇分公司)党委书记、副总经理,河北高速集团卓能有限公司法人,主要从事高速公路系统的智能化管理和数字化运营。
E-mail: 735262901@qq.com

崔洪军(1974-),男,河北定州人,博士,教授,博士生导师,2006年博士毕业于东南大学,主要从事交通系统可靠性分析、交通规划与管理、交通设施设计与交通安全、道路检测与养护技术等研究。
E-mail: cuihongjun@hebut.edu.cn

张左林(1999-),男,河北唐山人,博士研究生,2021年于河北工业大学获得学士学位,主要从事钙钛矿太阳能电池效率与稳定性研究。
E-mail: zuolin2024@126.com

陈聪(1990-),男,吉林长春人,博士,教授,博士生导师,2019年于吉林大学获得博士学位,研究方向为光伏与光电子集成器件,包括新型太阳能电池、NIR光电探测器和第三代半导体功率器件及钝化技术等。
E-mail: chencong@hebut.edu.cn